Numerical Analysis of Solids Mixing in Pressurized Fluidized Beds

ARTICLE *in* INDUSTRIAL & ENGINEERING CHEMISTRY RESEARCH · JANUARY 2010

Impact Factor: 2.59 · DOI: 10.1021/ie9014843

4 AUTHORS, INCLUDING:

Niels G Deen
Technische Universiteit Eindhoven
175 PUBLICATIONS **3,017** CITATIONS
SEE PROFILE

Hans A. M. Kuipers
Technische Universiteit Eindhoven
438 PUBLICATIONS **9,511** CITATIONS
SEE PROFILE

Numerical Analysis of Solids Mixing in Pressurized Fluidized Beds

Niels G. Deen,* Godlieb Willem, Gorter Sander, and J. A. M. Kuipers

Institute for Mechanics Processes and Control Twente (IMPACT), Faculty of Science and Technology, University of Twente, P.O. Box 217, NL-7500 AE Enschede, The Netherlands, and Dutch Polymer Institute, P.O. Box 902, 5600 AX Eindhoven, The Netherlands

In the production and processing of granular matter, mixing of solids plays an important role. Granular materials such as sand, polymeric particles, and fertilizers are processed in different apparatuses such as fluidized beds, rotary kilns, and spouted beds. In the operation of these apparatuses, proper mixing is essential, as it helps to prevent the formation of hot spots, off-specification products, and undesired agglomerates. In this article, we discuss various methods that are available to give quantitative information on the solids mixing state in granular systems based on a discrete description of the solids phase. We apply the different methods to two-fluid model simulations. It is found that some of these methods are grid-dependent; not reproducible; sensitive to macroscopic flow patterns; and/or able to calculate only overall mixing indices, rather than indices for each direction. We compare some methods described in the literature, and in addition, we propose two new methods that do not suffer from the disadvantages mentioned above. Simulations are performed for seven different operating pressures. It is found that mixing improves with operating pressure as a result of increased porosity in the dense phase.

Introduction

Gas fluidized beds are widely used in industry in various large-scale processes involving physical and/or chemical operations. The large specific surface areas of the solids in fluidized beds are beneficial for various operations, such as gas−solid reactions, cooling, and drying. In many cases, it is important that all particles be well-mixed so that all particles cool, react, or dry in a similar manner, to prevent hot-spot formation or agglomeration.

Solids mixing of granular materials has been researched widely. Because solids mixing is difficult to characterize experimentally, some groups use discrete element models (DEMs) or discrete particle models (DPMs) to investigate solids mixing behavior. McCarthy et al.[1] succeeded in validating their simulations with experiments, which indicates that modeling is a promising approach to describe solids mixing in detail.

In this work, we investigate the capabilities of four different methods, previously proposed by Godlieb et al.,[2,3] that can be used to calculate a mixing index from two-fluid model (TFM) simulations of fluidized beds. A mixing index (M) is used to quantify the state of mixedness of the system and is 0 or 1 for fully demixed and fully mixed conditions, respectively. The mixing index is also known as the entropy of mixing,[4] whereas Lu and Hsiau[5] called it the mixing degree, and Finnie et al.,[6] Asmar et al.[7] and Van Puyvelde[8] called it the mixing index. Although most authors try to determine the mixing index from DEM simulations, they use different methods: Schutyser et al.[4] calculated entropy based on entropy equations from molecular dynamics, whereas Mostoufi and Chaouki[9] used the "color" of a marked region (a spot) in the middle of the bed and measured the radius of the spot as a function of time. They were not able to calculate a mixing index. Lu and Hsiau[5] and Rhodes et al.[10] used the Lacey index[11] as a mixing index, as described later.

Two-fluid models or Euler−Euler models usually employ the kinetic theory of granular flow (KTGF) to close the equations for the particulate phase. Gidaspow[12] performed ground-breaking work to derive the KTGF, which is the basis of this work. TFMs can be used to determine mixing by employing two particulate phases, as shown by Darelius.[13] In this work, we use tracer particles that move with the interpolated velocity of the particulate phase. By using tracer particles, the same methods as used by Godlieb et al.[2,3] for analyzing DPM results can be used to analyze mixing from TFM simulation data. This has the great advantage that the mixing is decoupled from the number of particle phases that are solved in the TFM.

We test two new methods to quantify mixing: one based on the coloring of the 12 nearest neighbors of a particle and one based on the increasing distance of initially neighboring particles. In this work, we use the average-height method and Lacey's method, as well as the two newly proposed methods, to investigate solids mixing in a fluidized bed containing monodisperse polymeric particles at different operating pressures. In the first part of this article, the governing equations of the TFM are presented, followed by the various methods to characterize solids mixing. Subsequently, the results of the different methods applied to the simulation data are discussed, and conclusions are presented.

Model Description

Two-Fluid Model. In the two-fluid model (TFM), both the gas and solids phases are described as continuous interpenetrating fluids. The equations of motion for the gas phase are

$$\frac{\partial}{\partial t}(\varepsilon_f \rho_f) + (\nabla \cdot \varepsilon_f \rho_f \bar{u}) = 0 \tag{1}$$

$$\frac{\partial}{\partial t}(\varepsilon_f \rho_f \bar{u}) + (\nabla \cdot \varepsilon_f \rho_f \bar{u}\bar{u}) = -\varepsilon_f \nabla p - (\nabla \cdot \varepsilon_f \bar{\bar{\tau}}_f) - \bar{S}_p + \varepsilon_f \rho_f \bar{g} \tag{2}$$

The motion of the solids phase is described by

$$\frac{\partial}{\partial t}(\varepsilon_s \rho_s) + (\nabla \cdot \varepsilon_s \rho_s \bar{v}) = 0 \tag{3}$$

* To whom correspondence should be addressed. E-mail: N.G.Deen@utwente.nl.

10.1021/ie9014843

$$\frac{\partial}{\partial t}(\varepsilon_s\rho_s\bar{v}) + (\nabla\cdot\varepsilon_s\rho_s\bar{v}\bar{v}) = -\varepsilon_s\nabla p - (\nabla\cdot\varepsilon_s\bar{\bar{\tau}}_s) - \nabla p_s + \bar{S}_p + \varepsilon_s\rho_s\bar{g} \quad (4)$$

The interfacial momentum transfer is modeled by

$$\bar{S}_p = \beta(\bar{u} - \bar{v}) \quad (5)$$

where the interphase momentum-transfer coefficient, β, describes the drag of the gas phase acting on the particles, which is modeled with the relation proposed by van der Hoef et al.[14]

$$\beta = 18\frac{\mu_f}{d^2}\left[10\frac{\varepsilon_s^2}{\varepsilon_f} + \varepsilon_f^3\varepsilon_s(1 + 1.5\sqrt{\varepsilon_s})\right] \quad (6)$$

For the equation of state of the solids phase, the kinetic theory of granular flow (KTGF) is used. This theory was initially developed by Gidaspow[12] for multiphase systems involving particles. In addition to the continuity and Navier−Stokes equations, the granular temperature equation is solved for the particulate phase. The overall granular temperature is defined as

$$\Theta = \frac{1}{3}\langle\bar{C}_p\cdot\bar{C}_p\rangle \quad (7)$$

where

$$\bar{C}_p = \bar{c}_p - \bar{v} \quad (8)$$

Note that the particle velocity ($\bar{c}_p$) is decomposed into the local mean velocity ($\bar{v}$) and the fluctuation velocity component ($\bar{C}_p$).

The granular temperature is given by

$$\frac{3}{2}\left[\frac{\partial}{\partial t}(\varepsilon_s\rho_s\Theta) + (\nabla\cdot\varepsilon_s\rho_s\Theta\bar{v})\right] = -(p_s\bar{\bar{I}} + \varepsilon_s\bar{\bar{\tau}}_s):\nabla\bar{v} - \nabla\cdot(\varepsilon_s q_s) - 3\beta\Theta - \gamma \quad (21)$$

The KTGF closure equations that were used in this work can be found in Table 1. For details on the numerical implementation, we refer to the work of Goldschmidt et al.[15]

Tracer Particles. To investigate mixing with the TFM, one could define multiple solids phases with the same properties but different colors. Drawbacks of this approach are grid dependency, initial coloring dependency, and the inability to investigate subgrid mixing. An attractive alternative to the use of multiple solids phases is the use of tracer particles. As the motion of the solids phase is visualized by tracer particles, the same methods for characterizing mixing as used in discrete particle models can be applied.

By definition, tracer particles have no mass and follow the solids-phase velocity exactly. The velocity of the tracer particles is interpolated from the solids-phase velocity as follows

$$\bar{v}_p = D(\bar{x} - \bar{x}_m)\bar{v}_s \quad (22)$$

In this work, we use volume weighting (i.e., trilinear interpolation) for the interpolation

$$D(\bar{x} - \bar{x}_m) = \prod_i D(x_i - x_{m,i}) \quad (23)$$

where

$$D(x_i - x_{m,i}) = \begin{cases} 1 - \delta_i & \text{if } \delta_i \le 1 \\ 0 & \text{if } \delta_i > 1 \end{cases} \quad (24)$$

Table 1. KTGF Closure Equations

Phase Densities

$$\rho_f = \frac{Mp}{RT} \quad (9)$$

$$\rho_s = \rho_{s,0} \quad (10)$$

Stress Tensors

$$\tau_f = -\left\{\left(\lambda_f - \frac{2}{3}\mu_f\right)(\nabla\cdot\bar{u})I + \mu_f[(\nabla\bar{u}) + (\nabla\bar{u})^T]\right\} \quad (11)$$

$$\tau_s = -\left\{\left(\lambda_s - \frac{2}{3}\mu_s\right)(\nabla\cdot\bar{v})I + \mu_s[(\nabla\bar{v}) + (\nabla\bar{v})^T]\right\} \quad (12)$$

Solids Bulk and Shear Viscosities

$$\lambda_s = \frac{4}{3}\varepsilon_s\rho_s d_p g_0(1 + e)\sqrt{\frac{\Theta}{\pi}} \quad (13)$$

$$\mu_s = \mu_{s,c} + \mu_{s,k}\left\{\frac{\left[1 + \frac{4}{5}(1 + e)\varepsilon_s g_0\right]\left(1 + \frac{8}{5}\varepsilon_s g_0\right)}{\varepsilon_s g_0}\right\} \quad (14)$$

$$\mu_{s,c} = \frac{4}{5}\varepsilon_s\rho_s d_p g_0(1 + e)\sqrt{\frac{\Theta}{\pi}} \quad (15)$$

$$\mu_{s,k} = 1.016\frac{5}{96}\pi\rho_s d_p\sqrt{\frac{\Theta}{\pi}} \quad (16)$$

Pseudo-Fourier Energy Flux

$$\bar{q}_s = -\kappa\nabla\Theta \quad (17)$$

Solids Pseudoconductivity

$$\kappa = \kappa_{s,c} + \kappa_{s,k}\left\{\frac{\left[1 + \frac{6}{5}(1 + e)\varepsilon_s g_0\right]\left(1 + \frac{12}{5}\varepsilon_s g_0\right)}{\varepsilon_s g_0}\right\} \quad (18)$$

$$\kappa_{s,c} = 2\varepsilon_s\rho_s d_p g_0(1 + e)\sqrt{\frac{\Theta}{\pi}} \quad (19)$$

$$\kappa_{s,k} = 1.02513\frac{75}{384}\pi\rho_s d_p\sqrt{\frac{\Theta}{\pi}} \quad (20)$$

and

$$\delta_i = \frac{|x_i - x_{m,i}|}{\Delta x_i} \quad (25)$$

where δ_i is the dimensionless distance between the Eulerian position x_i and the Lagrangian position of the tracer particle $x_{m,i}$ in the x_i direction.

Methods for Characterizing Mixing

In this work, we use four different methods to obtain mixing indices from TFM data. Each of these methods is now briefly introduced.

Average-Height Method. The average-height method is the simplest of the investigated methods and is based on the average height of a group of colored particles. It is widely used for measuring segregation, for example, by Hoomans et al.[16] In the case of monodisperse systems, one-half of the particles are assigned a color, while all physical properties remain unchanged and are constant throughout the set of particles. Subsequently, the average position of all particles is monitored. Although the mixing behavior can, in principle, be investigated in all three directions, here, we explain only mixing in the vertical direction. In the first step of the algorithm, the vertical positions of all particles are sorted to determine the median height. Subsequently, the lower half of the particles is colored white, and the upper half is colored black. For each time step, the average height of the white particles can be calculated and normalized by the average height of all particles

$$\bar{z}_{\text{white}} = \frac{\frac{1}{N_{\text{white}}} \sum_{i \in \text{white}} z_i}{\frac{1}{N_{\text{all}}} \sum_{i \in \text{all}} z_i} \tag{26}$$

where $\bar{z}_{\text{white}}$ is the normalized average vertical position of the white particles. Notice that, initially, $\bar{z}_{\text{white}} = 0.5$ and, when the system fully mixed, it becomes 1.0. We now define the mixing index as

$$M = 2(\bar{z}_{\text{white}} - 0.5) \tag{27}$$

which means that, for $M = 0$, the system is fully demixed and, for $M = 1$, the bed is fully mixed.

This method can also be used to study lateral mixing. In those cases, the left and right or front and back parts are respectively colored white and black.

Lacey's Method. The Lacey index is based on statistical analysis and was developed by Lacey.[11] The variance S^2 for the concentration of the black particles in each cell is defined as

$$S^2 = \frac{1}{N-1} \sum_{i=1}^{N} (\phi_i - \phi_{\text{m}})^2 \tag{28}$$

where N is the number of cells in the bed containing particles, ϕ_i is the concentration of black particles in cell i, and ϕ_{m} is the average concentration of black particles in the bed.

S_0^2 and S_{R}^2 are defined as

$$S_0^2 = \phi_{\text{m}}(1 - \phi_{\text{m}}) \tag{29}$$

$$S_{\text{R}}^2 = \frac{\phi_{\text{m}}(1 - \phi_{\text{m}})}{n} \tag{30}$$

and represent the variances of the unmixed bed and the fully mixed bed, respectively. n is the average number of particles per cell.

The mixing index can be calculated as

$$M = \frac{S^2 - S_0^2}{S_{\text{R}}^2 - S_0^2} \tag{31}$$

Because of the use of grid cells, the Lacey index is grid-dependent. A coarse grid gives higher mixing indices, because, in that case, micromixing effects are neglected. A fine grid gives lower mixing indices, if only few particles are present in a cell. If only one particle is present in a cell, the system is always fully unmixed.

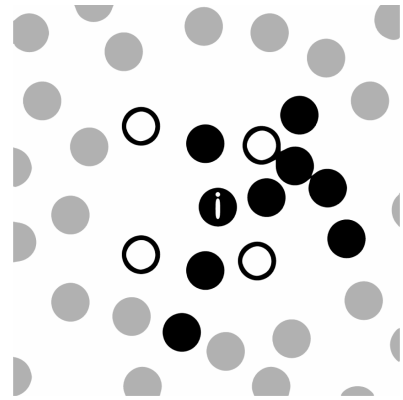

Figure 1. Illustration of the nearest-neighbors method. For the highlighted particle (i), the 12 nearest neighbors are shown. Four of them are white, and eight are black. Particles that are located farther away are colored gray and are not taken into account for this particle.

Nearest-Neighbors Method. Contrary to the average-height method, in which the overall average height of the particles is monitored, in the nearest-neighbor method, we evaluate the mixing in the vicinity of individual particles. In contrast to the Lacey index, the nearest-neighbor approach is grid-independent. Initially, we color one-half of the particles black, similarly to what is done in the average-height method. For each particle, we determine the 12 nearest-neighbor particles. If these particles have the same color as the particle under investigation, the system is unmixed, whereas if one-half of the nearest neighbors are colored differently, the system is fully mixed. This definition of the mixing index is expressed as follows

$$M = \frac{1}{N_{\text{part}}} \sum_{N_{\text{part}}} \frac{2n_{\text{diff}}}{n_{\text{nb}}} \tag{32}$$

where n_{diff} is the number of nearest neighbors colored differently and n_{nb} is the number of nearest neighbors.

Figure 1 shows an example for one individual particle, for which four neighboring particles have a different color (i.e., white). The mixing index for particle i is $(2 \times 4)/12 = 0.67$. The overall mixing index is the average over all particles.

Neighbor-Distance Method. The fourth method used in this work is based on the distance between initial neighbors. At a given time, the nearest neighbor is detected for each particle. Each particle and its nearest neighbor form a pair, and the center-to-center distance of the pair is monitored as time progresses. Initially, the distance is on the order of one particle diameter, and if the bed is fully mixed, it can increase up to the bed dimensions.

Figure 2 (top) shows the average distance between initial neighbors normalized with the particle diameter. Initially, it is just above one particle diameter, and after 1 s, it has increased up to 60 times the particle diameter. It is not a smooth curve, because bubbles let the bed expand and collapse, causing the distance between particles to increase and decrease with time. This effect introduces noise into the mixing measurement. Therefore, the distance is normalized by the distance of randomly selected particle pairs (gray line), resulting in a smooth mixing curve, unaffected by bed expansions, as can be seen in Figure 2 (bottom). Because the initial distance between neighbors is one particle diameter, this configuration

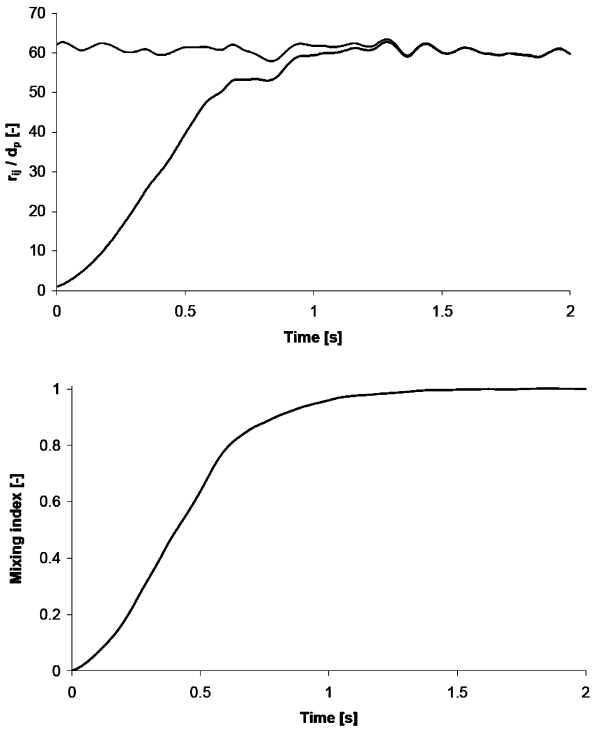

Figure 2. Top: Distance between initially nearest neighbors averaged over all pairs (black line) and average distance between random particles (gray line). Bottom: Corresponding mixing index determined with the neighbor-distance method.

is set to a mixing index of 0. The mixing index is thus expressed by the equation

$$M = \frac{\sum_{N_{\text{part}}} r_{ij} - d_p}{\sum_{N_{\text{part}}} r_{ik} - d_p} \tag{33}$$

where r_{ij} is the distance between particle i and its initially nearest neighbor j and r_{ik} is the distance between particle i and a randomly selected particle k.

The method just described can be used to calculate the mixing index for each direction. Note that, in that case, the initial distance between the partners *in one direction* can be less than a particle diameter. Some basic algebra shows that the average distance in one direction for two touching particles is $d_0 = 4d_p/\pi^2$.

The mixing index in the vertical direction for the neighbor-distance method is thus defined as

$$M_z = \frac{\sum_{N_{\text{part}}} r_{ij,z} - d_0}{\sum_{N_{\text{part}}} r_{ik,z} - d_0} \tag{34}$$

The mixing index for the horizontal direction x or y can be obtained by replacing subscript z by x or y, respectively.

Calculation of the Mixing Time. The mixing index is a valuable quantity for investigating the solids mixing process in fluidized beds. To compare different simulations in a simple way, the mixing index curve is condensed into a single value. We chose to use the 95% mixing time $t_{95\%}$, where the mixing index reaches a value of 0.95. To prevent noise from influencing the results, we used a dampened exponential function to fit the mixing index curve as follows

$$M_{\text{fit}} = 1 - Ae^{-\lambda t} \tag{35}$$

where A and λ are the amplitude and the damping coefficient, respectively. Each of these coefficients was obtained from the simulation data using a least-squares method. The fit as shown in Figure 3 accurately follows the trend of the curve. From this fit, we can calculate the mixing time at which the bed is 95% mixed, by solving eq 16 for t

$$t_{95\%} = \frac{-1}{\lambda} \ln\left(\frac{1 - 0.95}{A}\right) \tag{36}$$

Unfortunately, the average-height method shows periodic overshoots. This effect is caused by the macroscopic circulation patterns of the particles in the bed, as can be seen in Figure 4, which shows the mixing index obtained for the average-height method. Although $M = 1$ at 0.17 s, the bed is not fully mixed. At 0.31 s, the color pattern has been more or less inverted as a result of the bed circulation patterns, leading to an overshoot of $M = 1.6$. Eventually, after about 1.8 s, the overshoots have dampened out, and the bed is almost entirely mixed.

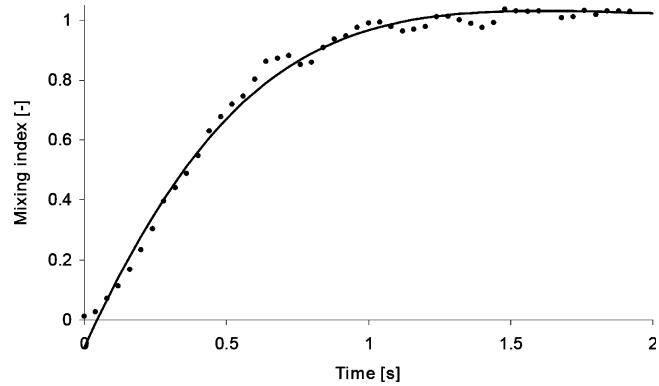

Figure 3. Lacey index fitted with a damped exponential function.

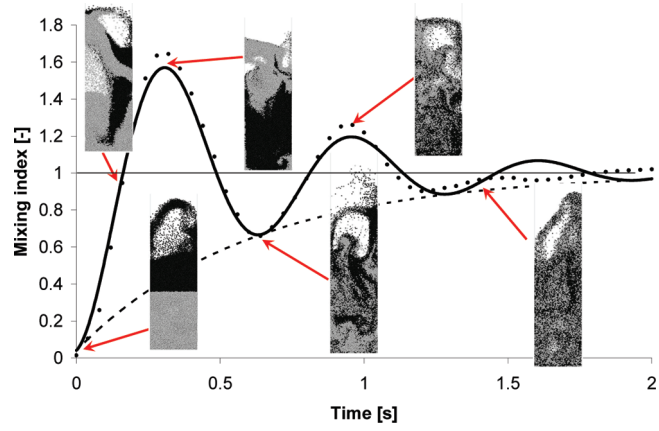

Figure 4. Mixing index versus time resulting from simulations (○), a fit of the data using eq 35 (− − −), and eq 37 (—). Images of the particles present in a slice in the center of the bed are shown as well.

Table 2. Gas Velocities for the Different Simulations

p (bar)	u_{mf} (m/s)	u_{sup} (m/s)
1	0.088	0.265
2	0.084	0.261
4	0.077	0.253
8	0.067	0.244
16	0.056	0.233
32	0.044	0.221
64	0.033	0.210

Because the mixing index is oscillating around a value of 1, it is hard to determine a mixing time; therefore, the curve is fitted with a damped harmonic oscillator

$$M_{\text{fit}} = 1 - Ae^{-\lambda t}\cos(\omega t) \tag{37}$$

where ω is the period of the oscillation. Now, we can calculate the 95% mixing time using the fit without the oscillator. By removing the periodic part from the fitted equation, we obtain an expression similar to eq 35 from which a 95% mixing time can straightforwardly be obtained.

Results

To enable a proper comparison between the simulations, a constant excess velocity (i.e., superficial velocity minus the minimum fluidization velocity) of 0.177 m/s was applied. The minimum fluidization velocity was calculated from the Ergun equation. The actual superficial gas velocities and minimum fluidization velocities are listed in Table 2.

Two-dimensional TFM simulations of a pressurized bubbling fluidized bed at a constant excess velocity (i.e., superficial velocity minus the minimum fluidization velocity) of 0.177 m/s were performed. The minimum fluidization velocity was calculated with the Ergun equation. The mixing behavior was analyzed for operating pressures ranging from 1 to 64 bar, similarly to the DPM simulations performed earlier by Godlieb et al.[2,3] The bed has dimensions of $D = 0.025$ m and $H = 0.15$ m and is filled with polymeric particles up to a static bed height of $H_0 = 0.025$ m. The polymeric particles have a diameter of $d_p = 0.5$ mm, a density of $\rho_s = 925$ kg/m^3, and a coefficient of restitution of $e = 0.8$. A computational stencil of 20×120 computational cells and a time step of 2×10^{-5} s were used. No-slip boundary conditions were used at the confining walls.

Unfortunately, the Lacey index mixing time could not be calculated for 64 bar, because the bed expanded too much, so that the number of particles per cell was no longer sufficient and the Lacey index no longer converged 1.

The results of the vertical and horizontal mixing times are shown in Figure 5. It was found that the obtained trends showed great similarities with the DPM results found by Godlieb et al.[2,3] (see Figure 6). Mixing times were found to decrease with increasing operating pressure. This phenomenon is due to an increased number of bubbles, which yields more chaotic particle movement at elevated pressure, hence improving the mixing. A deviation from this trend is noticed at higher pressures (especially 64 bar). This can be explained by analyzing snapshots of the particle positions (see Figures 7 and 8).

At a pressure of 64 bar, the bed tends to expand to almost twice the height at 2 bar. This has a large influence on mixing times, because the particles need to travel longer distances. The snapshots show that it takes more time for the bottom tracer particle to reach the top of the bed and, hence, to fully mix.

To assess the mixing irrespective of the bed expansion, we also analyzed the results for horizontal mixing. Because the horizontal pathway of the particles is bounded by the confining walls, bed expansion should have little effect on horizontal mixing. The results in Figure 5 (bottom) confirm this idea: the horizontal mixing times decrease at high pressure.

For vertical mixing, increasing the pressure has the effects that (i) the number of bubbles increases and chaotic movement in the bed *enhances* (micro-) mixing and (ii) the bed expansion increases the particle traveling distances and hence *decreases* (macro-) mixing. The first effect is dominant in the range of 1−8 bar, whereas the second effect is most important at high

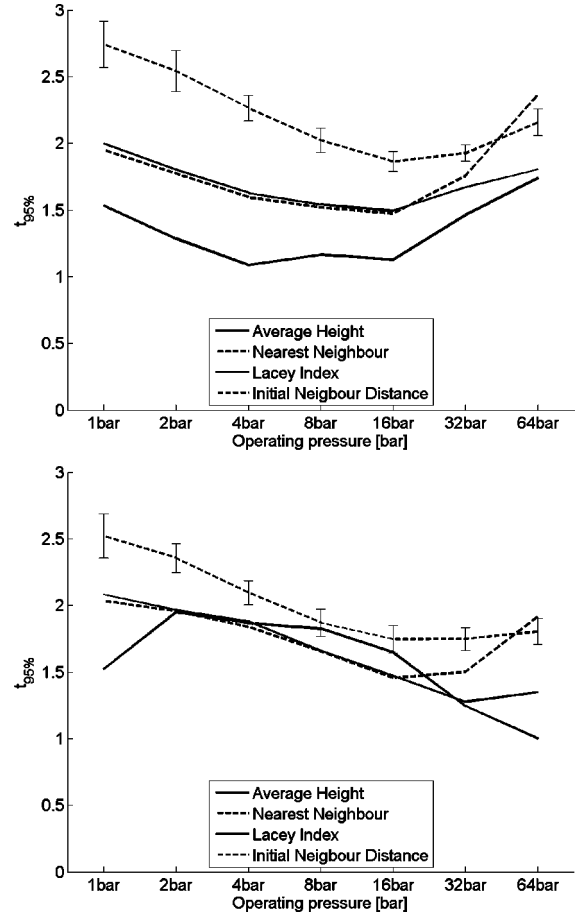

Figure 5. Mixing times versus operating pressure for vertical mixing (top) and horizontal mixing (bottom) from the TFM simulation. AH is average height, L is Lacey, NN is nearest neighbors, and ND is neighbor distance.

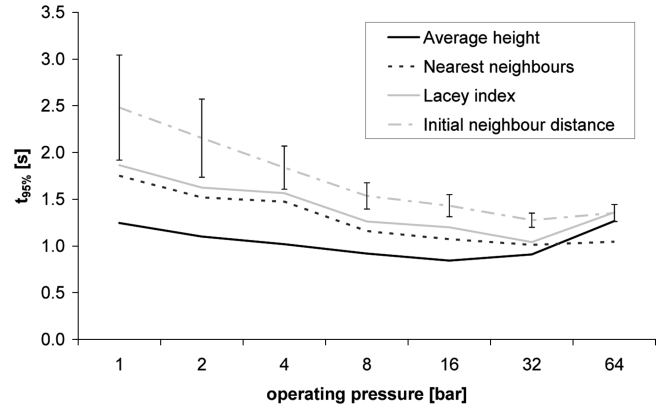

Figure 6. Mixing times versus operating pressure for vertical mixing from the DPM simulation (after Godlieb et al.[2,3]).

pressures. However, the results of the horizontal mixing do not show a smooth trend of decreasing mixing time at low pressures. After studying particle position snapshots, it was concluded that bed expansion has an important effect on horizontal mixing after all, especially at lower pressures. This can be explained as follows: The average solids motion takes the form of two counter-rotating vortices (see Figure 9). Horizontal motion is dominant only in the top and the bottom zones of the bed. It is in these zones that the mixing of colored particles starts (see Figure 10). Because mixing mostly happens at the top and bottom of the bed, the (expanded) bed height can influence horizontal mixing as well.

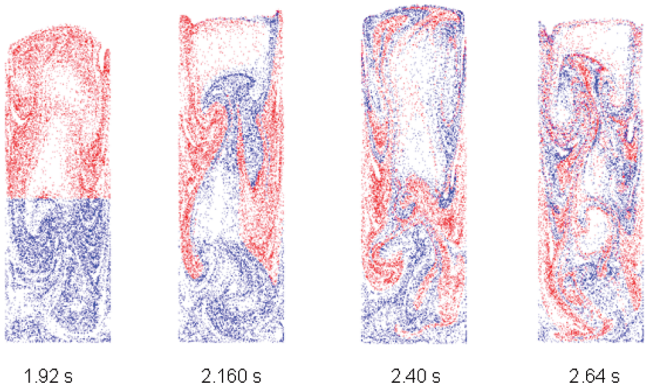

Figure 7. Snapshots of vertical mixing at 2 bar.

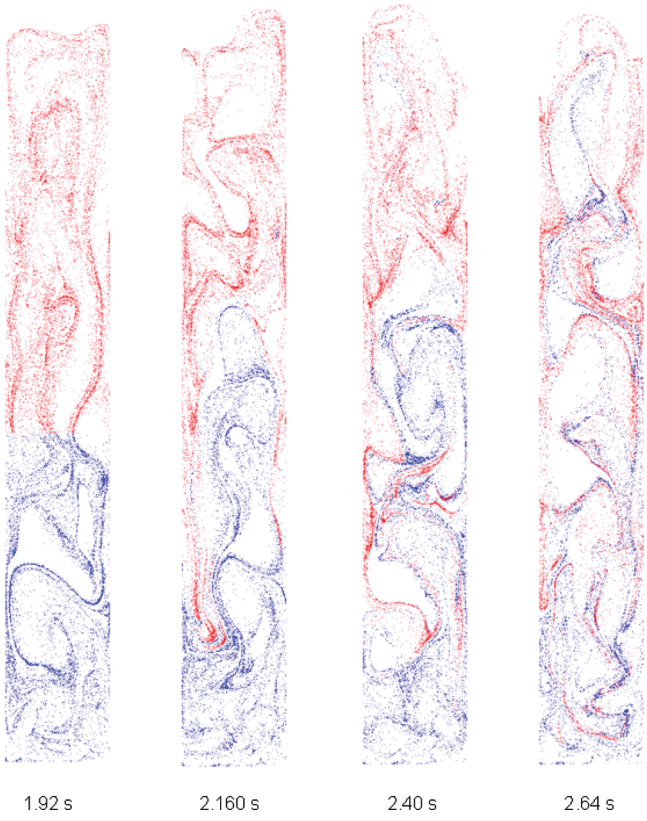

Figure 8. Snapshots of vertical mixing at 64 bar.

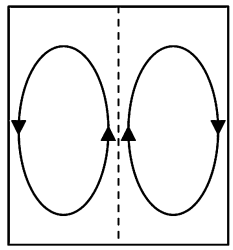

Figure 9. Schematic representation of average solids motion in a fluidized bed.

Extra simulations were performed to test the influence of bed height on the mixing times for vertical and horizontal mixing. For 2 and 32 bar, the initial bed height was reduced by 35%. Then again, mixing times were calculated. An average mixing time was determined by averaging the four mixing indices.

The results from these simulations are listed in Table 3 and show that reducing the bed height has similar effects for 2 and 32 bar on the vertical mixing time. Both are reduced by ~11%. For horizontal mixing, however, the results are different: the mixing time is less influenced than in vertical direction (only 6% reduction) for 32 bar, but it is reduced significantly for 2 bar (16%). This implies that (i) horizontal mixing occurs partially through a circular movement of particles in the bed, *decreasing* the mixing when a fluidized bed expands due to increasing pressure, and (ii) both factors direct horizontal motion and *increase* the mixing with increasing pressure, because of the more chaotic movement in the bed and increasing space between the particles.

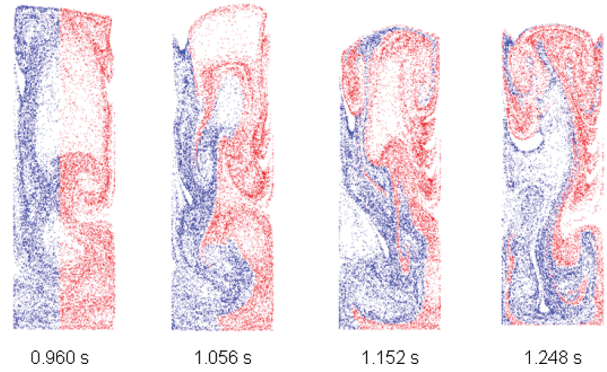

Figure 10. Snapshots of horizontal mixing at 1 bar.

Table 3. Average Vertical Mixing Times

p (bar)	H_0 (m)	vertical mixing time (s)	normalized vertical mixing time	horizontal mixing time (s)	normalized horizontal mixing time
2	0.025	1.93	1.0	2.21	1.0
2	0.016	1.69	0.88	1.85	0.84
32	0.025	1.69	1.0	1.52	1.0
32	0.016	1.49	0.89	1.43	0.94

For high pressures, the second effect is dominant, and therefore, horizontal mixing times are not affected by bed height as much as for lower pressures.

Pressure influences the hydrodynamics significantly, as can be seen in Figure 11, which shows the probability density function (PDF) of the porosity. For pressures below 32 bar, we see a clear peak around a porosity of 40−45%, representing the emulsion phase. Notice that, at maximum packing, the porosity is about 26%. Above 95%, we see some small peaks caused by bubbles. An intermediate area with porosities between 45% and 90% is formed in areas located around bubbles or in developing or collapsing bubbles. With increasing pressure, the porosity of the emulsion phase becomes less dense, and the

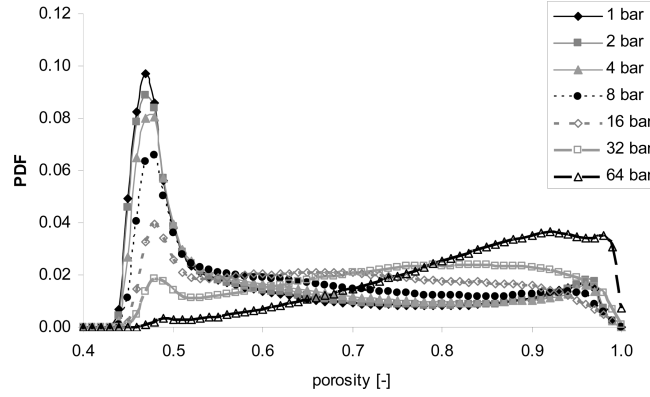

Figure 11. Time-averaged porosity distribution functions at different operating pressures.

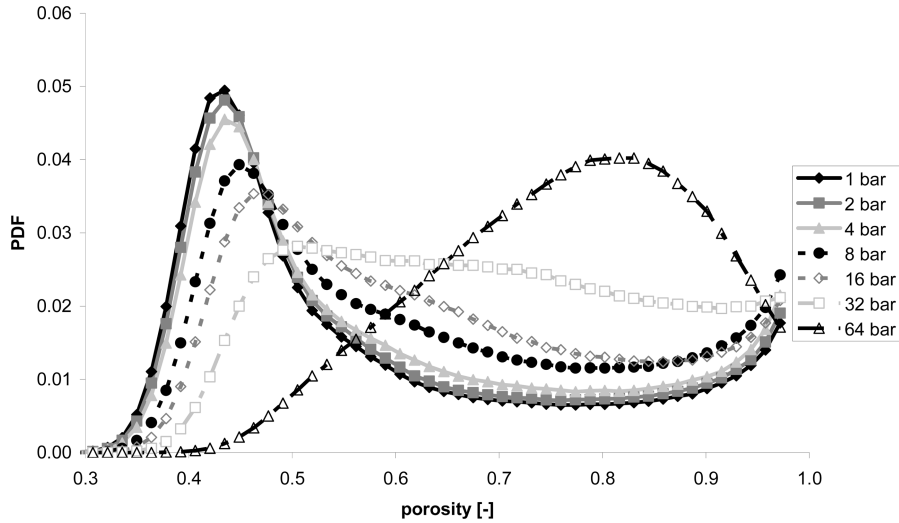

Figure 12. Time-averaged porosity distribution functions from DPM simulations (reproduced from Godlieb et al.[17] with permission).

bubbles contain more particles. The simulation at 64 bar does not show any peak for the emulsion phase. Hence, in that case, there is no clear distinction between the emulsion, intermediate, and bubble phases; instead, a new peak is formed around 90%. These results are qualitatively in close resemblance to the DPM results of Godlieb et al.,[17] which are shown for reference in Figure 12.

Conclusions

In this work, four different methods for analyzing solids mixing in two-fluid modeling are compared: the average-height method and Lacey's method, the nearest-neighbor method, and the neighbor-distance method. Each of these methods was used to characterize solids mixing in a fluidized bed containing monodisperse polymeric particles at different operating pressures.

The average-height method for analyzing particle mixing can provide valuable insight into overall mixing behavior in a fluidized bed. Although this method is very useful for visually monitoring mixing behavior, it has the disadvantage that there is a restricted number of diversity (depending on the amount of different colors used) of the particles. To determine a mixing index, it is important to know only whether a particle has color 1 or 2, and this restricts the first three methods in quantifying mixing behavior. The neighbor-distance method is the only method in which the mixing index does not depend on coloring, which makes it the method of choice to quantify solids mixing.

The TFM simulations show useful trends and great similarity with the DPM simulations that were performed earlier. The effects of increasing pressure on mixing behavior were determined for vertical and horizontal mixing. For vertical mixing the following observations were made:

(1) With increasing pressure, the number of bubbles increases, leading to more chaotic particle movement in the bed, which *enhances* vertical (micro-) mixing.

(2) Expansion of the bed increases particle traveling distances and *decreases* vertical (macro-) mixing.

For high increasing pressure, the second effect is dominant.

For horizontal mixing, the following conclusions were made:

(1) Horizontal mixing occurs partially through the circular movement of particles in the bed. Mixing *decreases* when a fluidized bed expands due to increasing pressure.

(2) Direct horizontal motion and mixing of particles *increase* with increasing pressure, because of the more chaotic movement in the bed and increasing space between the particles.

For increasing pressures, the latter effect is dominant, and therefore, horizontal mixing times are not as affected by bed height as for lower pressures.

Nomenclature

A = amplitude
d = diameter (m)
D = discrete Dirac delta function
Δt = time step (s)
F = force (kg m s^{-2})
g = gravitational acceleration (m s^{-2})
m = mass (kg)
M = mixing index
N = number of particles
p = pressure (N m^{-2})
r_{ij} = distance between particles i and j (m)
r_p = particle radius
S^2 = variance
$\bar{S}_p$ = sink term (kg m^2 s^{-1})
t = time (s)
u = gas velocity (m s^{-1})
v = solids velocity (m s^{-1})
V = volume (m^3)
x = X coordinate (m)
y = Y coordinate (m)
z = Z coordinate (m)

Greek Letters

β = momentum-transfer coefficient (kg s^{-1} m^{-2})
δ = dimensionless distance
ε = porosity
ϕ = particle concentration
γ = damping coefficient (s^{-1})
μ = viscosity (kg m^{-1} s^{-1})
ρ = density (kg m^{-3})
$\bar{\tau}_f$ = gas-phase stress tensor (kg m^2 s^{-1})
θ = granular temperature (m^2 s^{-2})
ω = period (rad s^{-1})

Subscripts

diff = different
f = fluid
fit = fitted
g = gas

i, j, k, m = particle numbers
M = mean
mf = minimum fluidization
n = normal
sup = superficial
t = tangential

Acknowledgment

This work is part of the Research Programme of the Dutch Polymer Institute (DPI) as Project #547.

Literature Cited

(1) McCarthy, J. J.; Khakhar, D. V.; Ottino, J. M. Computational studies of granular mixing. *Powder Technol.* **2000**, *109*, 72–82.

(2) Godlieb, W., Deen, N. G., Kuipers, J. A. M. Characterizing solids mixing in DEM simulations. In *Proceedings International Conference on Multiphase Flows (ICMF6)*; Sommerfield, M., Ed.; Technische Universität Darmstadt: Darmstadt, Germany, 2007.

(3) Godlieb, W., Deen, N. G., Kuipers, J. A. M. A discrete particle simulation study of solids mixing in a pressurized fluidized bed. In *Fluidization XII*; Berruti, F., Bi, X. T., Pugsley, T. S., Eds.; Engineering Conferences International: Brooklyn, NY, 2007; pp 751−758.

(4) Schutyser, M. A. I.; Padding, J. T.; Weber, F. J.; Briels, W. J.; Rinzema, A.; Boom, R. Discrete particle simulations predicting mixing behavior of solid substrate particles in a rotating drum fermenter. *Biotechnol. Bioeng.* **2001**, *75*, 666–675.

(5) Lu, L.-S.; Hsiau, S.-S. Mixing in vibrated granular beds with the effect of electrostatic force. *Powder Technol.* **2005**, *160*, 170–179.

(6) Finnie, G. J.; Kruyt, N. P.; Ye, M.; Zeilstra, C.; Kuipers, J. A. M. Longitudinal and transverse mixing in rotary kilns: A discrete element method approach. *Chem. Eng. Sci.* **2005**, *60*, 4083–4091.

(7) Asmar, B. N.; Langston, P. A.; Matchett, A. J. A generalised mixing index in distinct element method simulation of vibrated particulate beds. *Granular Matter* **2002**, *3*, 129–138.

(8) Van Puyvelde, D. R. Comparison of discrete elemental modelling to experimental data regarding mixing of solids in the transverse direction of a rotating kiln. *Chem. Eng. Sci.* **2006**, *61*, 4462–4465.

(9) Mostoufi, N.; Chaouki, J. Local solid mixing in gas−solid fluidized beds. *Powder Technol.* **2001**, *114*, 23–31.

(10) Rhodes, M. J.; Wang, X. S.; Nguyen, M.; Stewart, P.; Liffman, K. Study of mixing in gas-fluidized beds using a DEM model. *Chem. Eng. Sci.* **2001**, *56*, 2859–2866.

(11) Lacey, P. Developments in theory of particulate mixing. *J. Appl. Chem.* **1954**, *4*, 257.

(12) Gidaspow, D. *Multiphase Flow and Fluidization: Continuum and Kinetic Theory Descriptions*; Academic Press: Boston, MA, 1994.

(13) Darelius, A.; Rasmuson, A.; van Wachem, B.; Niklasson Bjørn, I.; Folestad, S. CFD simulation of the high shear mixing process using kinetic theory of granular flow and frictional stress models. *Chem. Eng. Sci.* **2008**, *63*, 2188–2197.

(14) van der Hoef, M. A.; Beetstra, R.; Kuipers, J. A. M. Lattice-Boltzmann simulations of low-Reynolds-number flow past mono- and bidisperse arrays of spheres: Results for the permeability and drag force. *J. Fluid Mech.* **2005**, *528*, 233–254.

(15) Goldschmidt, M. J. V.; Kuipers, J. A. M.; van Swaaij, W. P. M. Hydrodynamic modeling of dense gas-fluidised beds using the kinetic theory of granular flow: Effect of coefficient of restitution on bed dynamics. *Chem. Eng. Sci.* **2001**, *56*, 571–578.

(16) Hoomans, B. P. B.; Kuipers, J. A. M.; van Swaaij, W. P. M. Granular dynamics simulation of segregation phenomena in bubbling gas-fluidised beds. *Powder Technol.* **2000**, *109*, 41–48.

(17) Godlieb, W.; Deen, N. G.; Kuipers, J. A. M. On the relationship between operating pressure and granular temperature: A discrete particle simulation study. *Powder Technol.* **2008**, *182*, 250–256.

Received for review September 21, 2009
Revised manuscript received December 2, 2009
Accepted December 2, 2009

IE9014843